Modelling the impact of high-rise buildings in urban areas on precipitation initiation

M. G. D. Carraça[1,2] and C. G. Collier[2]*

[1] *C.G.E., Department of Physics, University of Évora, 7000, Portugal*
[2] *Centre for Environmental Systems Research, School Of Environment and Life Sciences, University of Salford, Greater Manchester, M5 4WT, UK*

ABSTRACT: The impact of urban areas upon precipitation distribution has been studied for many years. However, the relative importance of the distribution and type of surface morphology and urban heating remains unclear.

A simple model of the surface sensible heat flux is used to explore the impact of urban heterogeneity. Sensitivity experiments are carried out to test the validity of the model, and experiments with a schematic urban morphology are used to investigate the impact of different types of building arrays. It is found that high-rise buildings over relatively small areas may have just as much impact as somewhat lower buildings covering a much larger area. The urban area produces considerable spatial variation in surface sensible heat flux. Data from a C-band radar located to the north of Greater Manchester provides evidence that convective cells may be initiated by the sensible heat flux input generated by the high-rise buildings in the city centre when the atmospheric boundary layer is unstable. Copyright © 2007 Royal Meteorological Society

1. Introduction

Among the causes ascribed to the modification of precipitation induced by urbanization (Shepherd *et al.*, 2002), most studies suggest that dynamic forcing (destabilization associated with the heat island and surface roughness) is the most significant (e.g. Baik *et al.*, 2001; Guo *et al.*, 2006), more so than microphysical or moisture enhancement. Urban areas modify boundary layer processes mostly through the production of an urban heat island, and by increasing turbulence through locally enhanced roughness (for a review see Collier, 2006). Results of numerical studies (e.g. Thielen *et al.*, 2000; Shepherd, 2002; Rozoff *et al.*, 2003; Shepherd, 2005) show the impact of the surface sensible heat flux and roughness of urban surfaces on convective rain. Thielen and Gadian (1997) described a numerical study of the influence of topography and urban heat island effects on the outbreak of convective storms under unstable meteorological conditions. Analysis of data from convective storms in northern England confirmed that the combination of effects such as sea breezes, elevated terrain and the presence of large cities has an influence on the initiation and development of convective storms. The results of the numerical study show that the presence of the Pennines, a north–south-oriented ridge, could influence the initiation of convection due to its long Sun-facing slopes, and to a lesser degree forced lifting along these slopes. The inclusion of urban heat island effects produced enhanced and prolonged convection, particularly downwind of the major urbanized areas.

A comparison of the two average annual rainfall maps covering NW England for 1941–1970 and 1961–1990 (Met. Office, UK) suggests an increase in precipitation over the westerly suburbs of Greater Manchester. Considering the expansion of urbanization during the past 50 years with a significant increase in high-rise buildings in the early 1970s, it is reasonable to consider whether or not these differences in rainfall may be attributed to urban development. However, it may be that surface heterogeneity also impacts local wind flows, as described by Segal and Arritt (1992), leading to different rainfall regimes. The possible impact of global climate change may also be a factor in assessing changes over a period of many tens of years.

An estimate, based on the analysis of Shaw (1962), of the origins of precipitation in northern England shows that a considerable proportion (34–50%) of the total precipitation over the region of Greater Manchester is of convective origin. It may be anticipated that urban areas should have some impact on the initiation of this type of rainfall, which is reflected in the average annual rainfall distribution for the area.

---

* Correspondence to: C. G. Collier, Centre for Environmental Systems Research, School Of Environment and Life Sciences, University of Salford, Greater Manchester, M5 4WT, UK.
E-mail: c.g.collier@salford.ac.uk

In this paper, some results from a study of the influence of an urban area on convective clouds and precipitation are presented. Of particular interest is the degree to which spatial variations of surface heterogeneity, notably in the present work from high-rise buildings, impact these phenomena, and whether the processes involved can be represented appropriately within a single-column model of surface energy balance applied on a rectangular grid.

A numerical scheme is presented on the basis of several published systems, principally Grimmond and Oke (1999) and Voogt and Grimmond (2000), and is developed to derive fields of surface sensible heat flux, for a range of wind and temperature, over an urban area (Section 2). In Section 3, results of model tests are discussed and in Section 4 a case study in Greater Manchester is analysed. In Section 5, we compare the sensible heat flux fields derived in Section 4 with integrated rainfall fields derived from C-band radar data. Finally, some concluding remarks are presented in Section 6.

The objective is to apply the model for the Manchester urban area to convective daytime summer conditions. These are conditions for which we anticipate that the urban morphology will modify the distribution of sensible heat flux, and influence convective developments.

2. Modelling

In this section, a numerical scheme is described for deriving fields of surface sensible heat flux for a range of wind and temperature inputs over an urban area. The model is formulated initially for Greater Manchester, in a study area of 24×24 km, with a grid resolution of 1×1 km, where the bulk equations are used and the model parameters are specified as averages over each grid square.

The surface sensible heat flux, Q_H, over the urban area is calculated by a resistance-type formulation using the difference between the radiometric surface temperature, T_R, and air temperature, T_a, (Grimmond and Oke, 1999; Voogt and Grimmond, 2000):

$$Q_H = \rho c_p \frac{(T_R - T_a)}{r_H} \qquad (1)$$

$$r_H = \frac{1}{ku_*}\left[\ln\left(\frac{z_S - z_D}{z_{0M}}\right) - \Psi_H\right]$$
$$+ \frac{1}{ku_*}\ln\left(\frac{z_{0M}}{z_{0H}}\right) \qquad (2)$$

$$L = \frac{-u_*^3 \rho c_p T_a}{kg Q_H} \qquad (3)$$

$$u_* = ku\left[\ln\left(\frac{z_S - z_D}{z_{0M}}\right) - \Psi_M\right]^{-1} \qquad (4)$$

Here, the parameter g (9.8 m s^{-2}) is the acceleration due to gravity, ρ (1.2 kg m^{-3}) is the air density, c_p (1004 J kg^{-1} K^{-1}) is the specific heat of the air at constant pressure and k (0.4) is von Karman's constant.

In this formulation, Q_H is the surface sensible heat flux, r_H is the resistance to heat transfer from a surface at temperature T_R to an atmospheric level at temperature T_a, L is the Monin–Obukhov length, u_* is the friction velocity, z_D is the zero-plane displacement length, z_{0M} is the roughness length for momentum, z_{0H} is the roughness length for heat and Ψ_M and Ψ_H are the stability correction functions for momentum and heat respectively.

Input meteorological variables used in the model are T_R, T_a and the wind velocity is u. T_a and u are typically measured several metres above the surface, at the measurement height, z_S, in the inertial sub-layer where the Monin–Obukhov similarity theory (MOST) is valid. Although the validity of MOST in the atmospheric boundary layer has been questioned (Fisher, 2002), the surface sub-layer is usually studied within the framework of MOST. This forms the basis of the model to be used later to explore the impact of the heterogeneity of the urban canopy.

Input roughness parameters are the building height, z_H, and the frontal area index, λ_F. Over built-up areas, z_H and λ_F were derived from analysis of surface form according to the Grimmond and Oke (1999) methodology, while for natural surfaces these roughness parameters were estimated using reference tables given in the literature (e.g., Brutsaert, 1982; Wieringa, 1993; Grimmond et al., 1998; Grimmond and Oke, 1999).

The zero-plane displacement length, z_D, and roughness length for momentum, z_{0M}, are estimated as a function of building height, z_H, and frontal area index, λ_F, using the Raupach (1994, 1995) method. The roughness length for heat, z_{0H}, is determined as a function of z_{0M}, using the formulation proposed by Brutsaert (1982) for bluff-rough surfaces.

Stability corrections for momentum, Ψ_M, and heat, Ψ_H, are the Paulson (1970) stability functions. The Dyer (1974) equations modified by Hogstrom (1988) are used to calculate Ψ_M, when $L < 0$, and Ψ_H. The van Ulden and Holtslag (1985) equation is used to calculate Ψ_M, when $L > 0$. Q_H, u_* and L (or the stability functions) are determined by an iteration of Equations (1)–(4).

A useful approach in describing an urban energy budget is to consider a near-surface active layer (urban canopy) or control volume, whose top is set at, or above, the roof level and its base at the depth of zero net ground heat flux over the chosen time scale or period (Oke, 1987). In the present case, the top is set at the measurement height, z_S, in the inertial sub-layer. Using this approach, one can neglect the extremely complex spatial arrangement of individual canopy elements as energy sources or sinks. The control volume, or box, formulation considers only energy fluxes through its top. The internal heat storage associated with all the canopy elements, the surrounding air and the ground, and internal heat sources can be represented as equivalent fluxes through unit area of the top of the box.

3. Model tests

3.1. Sensitivity tests of the numerical model

3.1.1. Data

The model has been evaluated for the main situation of interest, namely atmospheric convective conditions over the Manchester, UK, region, which occur during daytime, typically in springtime and summer. On the other hand, in order to simplify the analysis of the tests, the synthetic examples studied (a total of 120) were organized into five groups (A, B, C, D, E) in such a way that in each group the input values are the same for all variables, except for one of them as follows:

(A) $z_H = 6$ m, $u = 1.5$ ms^{-1}, $T_R = 303$ K, $T_a = 293$ K and $\lambda_F = 0.01, 0.03, \ldots, 0.45$ or 0.47;
(B) $\lambda_F = 0.2$, $u = 1.5$ ms^{-1}, $T_R = 303$ K, $T_a = 293$ K and $z_H = 0.5, 1.0, \ldots, 11.5$ or 12.0 m;
(C) $\lambda_F = 0.2$, $z_H = 6$ m, $T_R = 303$ K, $T_a = 293$ K and $u = 0.5, 1.0, \ldots, 11.5$ or 12.0 ms^{-1};
(D) $\lambda_F = 0.2$, $z_H = 6$ m, $u = 1.5$ ms^{-1}, $T_a = 293$ K and $T_R = 274, 276, \ldots, 318$ or 320 K;
(E) $\lambda_F = 0.2$, $z_H = 6$ m, $u = 1.5$ ms^{-1}, $T_R = 303$ K and $T_a = 280, 281, \ldots, 302$ or 303 K.

In all the cases, the measurement height was taken as $z_S = 20$ m.

3.1.2. Results

The model is capable of providing estimates of the surface sensible heat flux, Q_H, with a precision of 1×10^{-4} Wm^{-2} (the model iterations are terminated when this value of precision is reached). If a higher precision is used, the computations are subject to larger truncation errors. Model output values for $z_D, z_{0M}, z_{0H}, \ldots, L, u_*$ and Q_H are derived.

Figure 1 shows some results of model tests for z_{0M} and Q_H, using the input values specified in the previous subsection. Each point on the curves represents a complete model run using a specific set of input values, a total of 24 for each curve. Each curve relates one output parameter (z_{0M} or Q_H) to one input variable; all the other input variables are kept constant. For example, curve A of Figure 1(b) shows the variation of Q_H as λ_F increases from 0.01 to 0.47, at intervals of 0.02, while the value of all the other input parameters is the same for all the points of this curve ($z_S = 20$ m, $z_H = 6$ m, $u = 1.5$ ms^{-1}, $T_R = 303$ K, $T_a = 293$ K). The x coordinate relates to the input parameters variability range defined in the previous subsection and indicated on the box below each graph.

For the range of typical input values used, the model behaves reasonably for slightly stable to unstable conditions. However, as expected, the model fails for the stable conditions represented by points D1–D9, where $z_S > L$, and does not converge for points C8 and D11, which are cases where there is a discontinuity of the stability functions. These discontinuities are a consequence of the established criteria for being near neutral stability: $|\zeta = (z_S - z_D)/L| < 0.1$, where $\Psi_M = \Psi_H = 0$.

A discontinuity is also observed between points A15 and A16, in this case due to the different behaviour of the roughness parameter z_{0M} for values of $\lambda_F > 0.29$. The value $\lambda_{F\,max}$ (0.29) can be interpreted as the onset of 'over sheltering', the point at which adding further roughness elements merely shelters one another (Raupach, 1994). After this point, the roughness z_{0M} is seen to decrease, yet the heat flux increases (Q_H).

3.2. Experiments on spatial variations of urban roughness

In order to identify the comparative impact of surface roughness *versus* local heating effects more clearly, some experiments using a stylized representation of the urban area have been carried out (Figure 2).

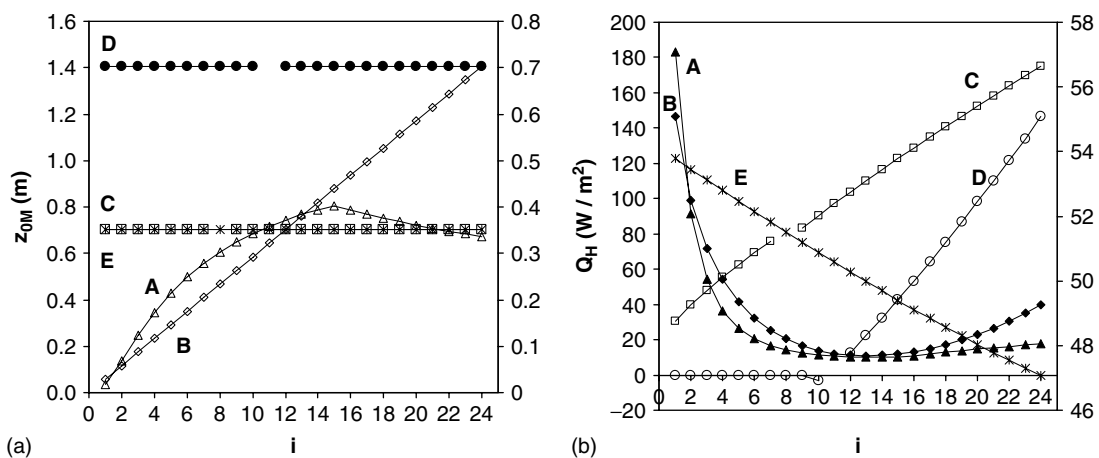Figure 2(a) shows model results of surface sensible heat flux, Q_H, for two wind speeds (3 and 10 ms^{-1}).

Figure 1. The graphs show some model results, for z_{0M} (a) and Q_H (b), using the input values discussed in the text. Each curve (A, B, C, D, E) relates to a different input variable, λ_F, z_H, u, T_R or T_a, while all others are kept constant. The x coordinate relates to the input variability range: λ_F (0.1–0.47), z_H (0.5–12 m), u (0.5–12 ms^{-1}), T_R (274–320 K) and T_a (280–303 K). (Filled symbols refer to the right y-axis, open symbols to the left y-axis.).
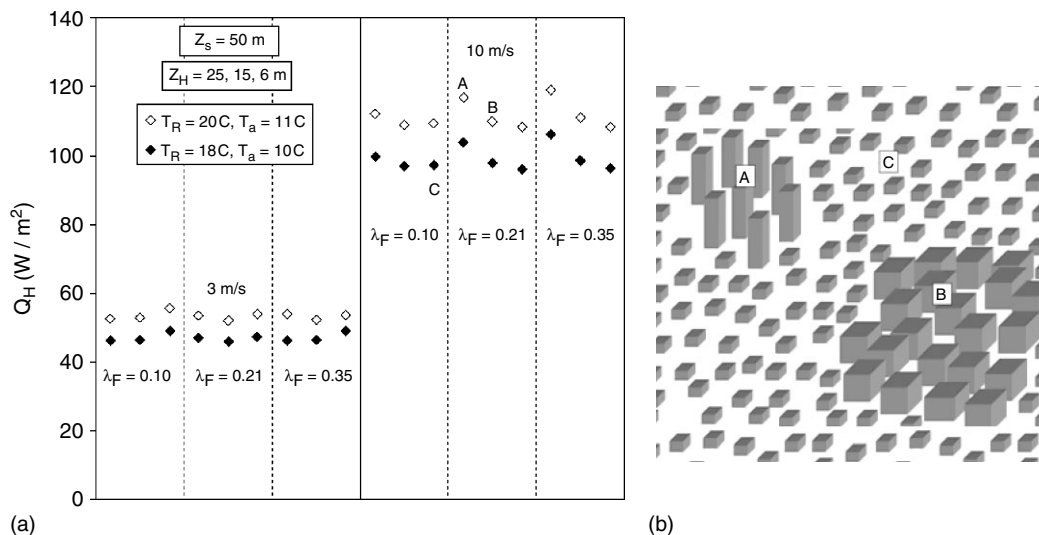
Figure 2. (a) Surface sensible heat flux results, Q_H, of a modelling experiment for two wind speeds ($u = 3$ and $10\ ms^{-1}$) and two vertical temperature gradients: $T_R = 20\,°C$, $T_a = 11\,°C$ and $T_R = 18\,°C$, $T_a = 10\,°C$ (open and filled symbols). Each point represents a complete model run using a specific set of input values, which are indicated on the graph. The measurement height, $z_S = 50$ m, is the same for all the cases, but three different building heights are considered: $z_H = 25$, 15 and 6 m. Here, points A, B and C relate to the urban area represented in (b); (b) Schematic representation of the distribution of roughness over an urban area loosely resembling a part ($5 \times 5\ km^2$) of Greater Manchester.

For both wind situations, three frontal area index values have been considered ($\lambda_F = 0.10$, 0.21 and 0.35), and for each of these cases three possible building height values ($z_H = 25$, 15 and 6 m) were used. In all the cases, the measurement height was the same, $z_S = 50$ m. This modelling experiment was carried out for two vertical temperature gradients (filled and open symbols).

The initial model results in Figure 2(a) show the impact of roughness and vertical temperature gradient on the spatial distribution of the surface sensible heat flux, Q_H. For example, considering the urban area represented in Figure 2(b), it can be seen that the area of uniform low buildings (C) has a lower sensible heat flux than those areas (A and B) which have higher roughness. However, interestingly, the area of high-rise buildings close together (A) produces almost the same sensible heat flux as the area (B) having lower buildings covering a much larger area than the high-rise buildings (A). This is investigated further, in the next section using the actual roughness distribution of Greater Manchester.

4. Case studies

4.1. Model input data

The model is implemented over Greater Manchester on a study domain of $24 \times 24\ km^2$, and grid of $1 \times 1\ km^2$ resolution. The study area comprises Manchester city centre and the major suburbs of Salford and Stockport, Manchester International Airport and some non-urbanized areas located mostly to the east and south. The terrain is quite flat; to the east it is bounded by the Pennines, the most significant feature in the region, but in the other directions, principally to the west, there are no significant relief features (Figure 3). The model is applied to the Greater

Manchester study area for selected study days. Here, two cases are presented, on the 14 and 21 June 2004.

Figure 4 shows differences between radiometric surface temperature, T_R, and air temperature near the surface, T_a, over Greater Manchester on some clear sky days. The data refer to a particular hour of the day, between 1155 and 1355 UTC, depending on the time of the satellite (Terra or Aqua) overpass available for each specific day. The radiometric surface temperature values, T_R, were obtained from satellite observations over Greater Manchester using the MODIS/Terra and MODIS/Aqua Land Surface Temperature/Emissivity [modis-land.gsfc.nasa.gov] (5 min, 1 km) data.

In Figure 4, the air temperature observations are obtained from different sources. The values referred to as Ta_SalfordUni, 20 m are given by an automatic weather station (AWS) installed at Salford University on the top of the 20 m high Telford building. On the other hand, the values referred to as Ta_Salford, 5 m are provided by an AWS situated in Salford and are available on-line [http:\\www.wunderground.com]. The observations from the AWS at Manchester airport, Ta_MxAirport, 2 m, are provided by the UK Met Office [www.wunderground.com, www.metoffice.gov.uk, or weather.noaa.gov]. Finally, Ta_UMIST, 50 m are air temperature observations from an AWS at the top of the 50 m high Sackville building in central Manchester, provided by the University of Manchester Atmospheric Science Research Group. The radiometric temperatures, derived from satellite data, represent the surface 'skin' temperature and are, on average, about 7 °C higher than the air temperatures.

Figure 5 shows the air temperature and wind observations on the 14 and 21 June 2004 from different sources as in Figure 4, except that for these days the
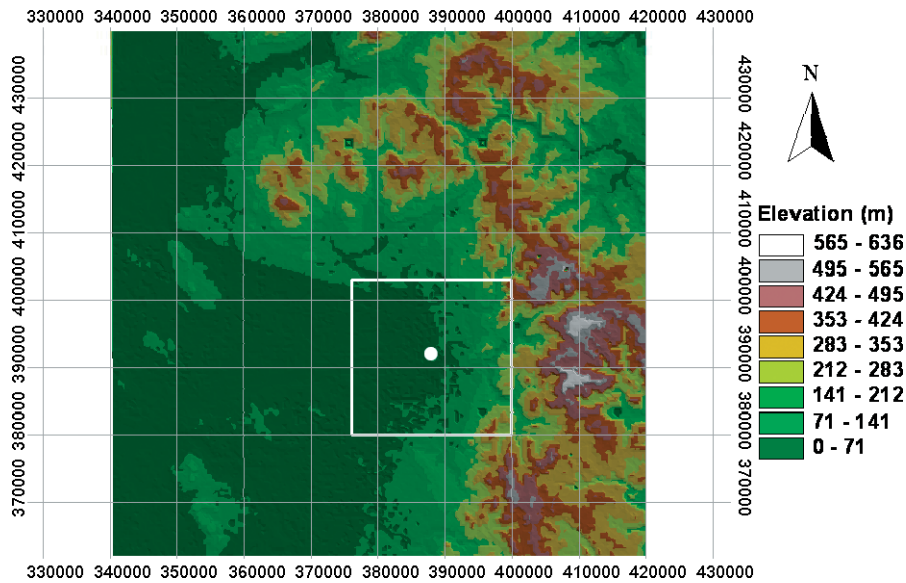
Figure 3. Relief in the Manchester region. The white square delimits the Greater Manchester study area of 24×24 km^2. The coordinates X and Y are the UK National Coordinates. The legend on the right-hand side refers to the values of the height above sea level expressed in metres.
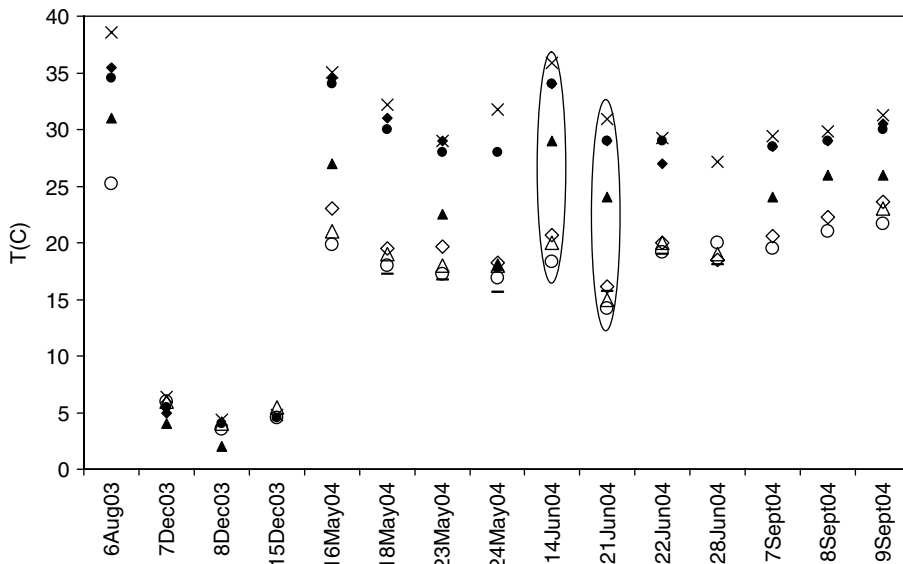

Figure 4. Air temperature (T_a) near the surface and radiometric surface temperature (T_R) over Greater Manchester around 12 UTC on some clear sky days (dates on x-axis). The air temperature data near the surface, T_a, were obtained from several sources (–Ta_SalfordUni, 20 m; ○Ta_Salford, 5 m; ◇Ta_UMIST, 50 m; △Ta_MxAirport, 2 m). The radiometric surface temperature at these sites, T_R, was obtained from satellite data (✕TRmax, ●TR_Salford, ◆ TR_Manchester, ▲TR_MxAirport).

AWS observations on the top of the 20-m-high building at Salford University are not available. For the 14 June observations of the air temperature (T_a) from a thermocouple located at this site are shown instead. Also, sonic measurements of virtual temperature and wind speed (T_v and u) are presented.

Because the air temperature data provided by the different sources were taken under different conditions, different measurement heights and different morphologic characteristics of the surrounding area, it is not easy to relate them. However, the air temperature values fell in quite a narrow range and, in the two study days, we decided to consider the same input value over the entire

domain, namely the value observed at Manchester Airport ($T_a = 293$ K; 288 K).

The wind speeds at the different sites (provided by the same sources as air temperature) were observed under different conditions, and in this case, quite a wide range of values is obtained. Thus, we assume that the values observed at Manchester airport ($u = 5.8$ ms^{-1}; 3.6 ms^{-1}), which are measured under standard conditions, can be used for our entire study domain. The mean wind direction in these study cases is northwest, which provides quite good conditions for the model evaluation, since there are no significant orographic obstacles in this direction (Figure 3).
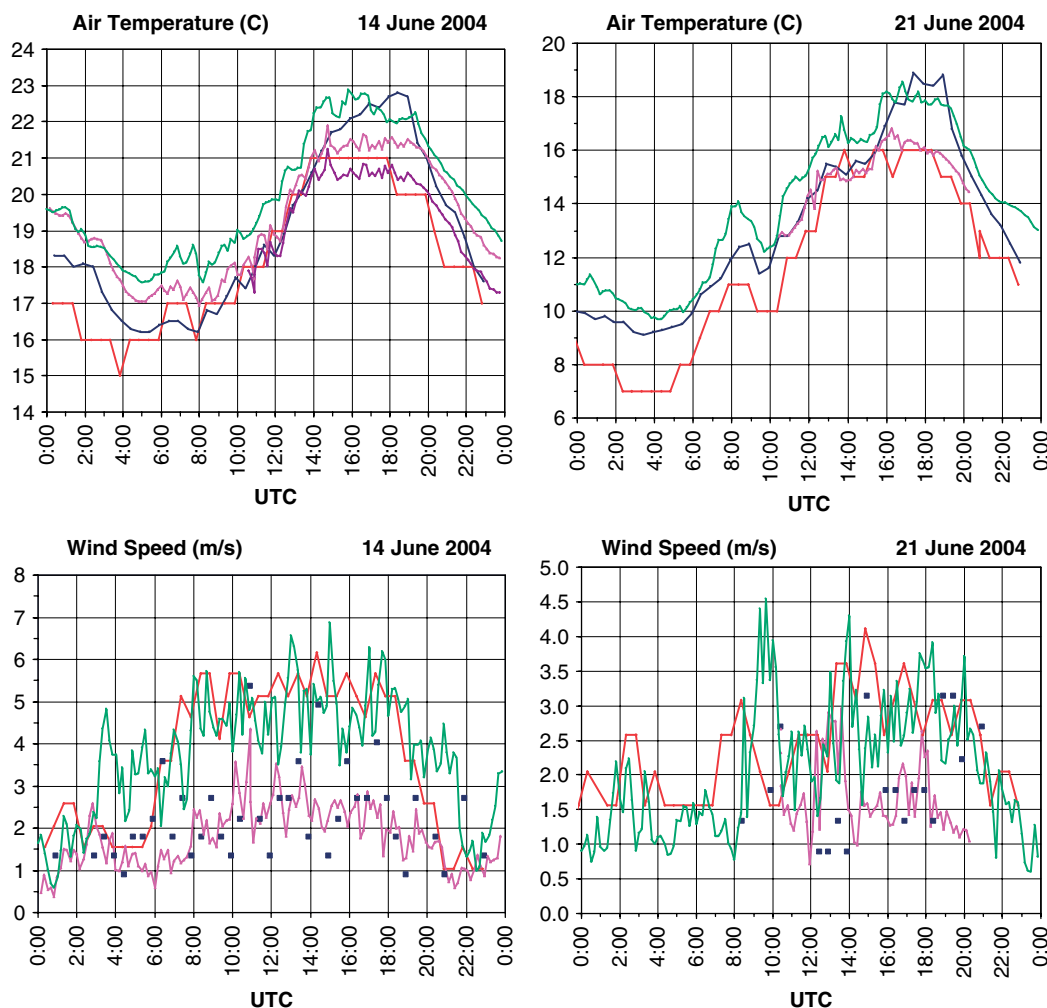
Figure 5. Air temperature, T_a, and wind speed, u, observations on the 14 and 21 June 2004 from different sources over Greater Manchester (—— Ta_MxAirport, 2 m, —— Ta_Salford, 5 m, —— Ta_UMIST,50 m, —— Tv_SalfordUni, 20 m, —— Ta_SalfordUni, 20 m; —— u_MxAirport, 10 m, ● u_Salford, 7 m, —— u_UMIST, 50 m, —— u_SalfordUni, 20 m).

Figure 6 shows the spatial distribution of the radiometric surface temperature, T_R, over Greater Manchester for the 24×24 km^2 area of interest, on the clear sky study day of 14 June 2004 at 1250 UTC, and on the cloudy day of 21 June 2004 at 1300 UTC. The radiometric surface temperature values, T_R, shown in Figure 6, were obtained from satellite observations over Greater Manchester using the MODIS/Terra MODIS/Aqua Land Surface Temperature/Emissivity [modis-land.gsfc.nasa.gov, last accessed on 11/10/2004] (5 min, 1 km) data. The values of T_R presented in Figure 4 were extracted from images similar to the examples given in Figure 6.

To implement the model, besides the weather data, surface morphology data need to be obtained for the study area. A surface morphologic database for Greater Manchester has been developed from analysis of digital elevation data, aerial photography, maps and field surveys. Model input roughness parameters, building height, z_H, and the frontal area index, λ_F, were estimated from digitised georeferenced data of the surface elements provided by the Environment Agency and the Cities Revealed User Group (for a detailed explanation see Carraça and Collier, 2006). The values so derived were comparable

with previously published work such as that described by Ellefsen (1990–1991). The values of z_H and λ_F obtained for the Greater Manchester study area are shown in Figure 7(a) and (b) respectively.

The input values used in the two case studies and described in the previous paragraphs are summarized in Table I.

Table I. Model input data used for the two case studies over the entire domain.

| 14 June 2004 case	21 June 2004 case
$T_a = 293$ K and $u = 5.8$ ms^{-1} Spatial distribution of T_R, from satellite imagery at 1250 UTC as shown in Figure 6(a). Spatial distribution of z_H and λ_F as shown in Figure 7(a) and (b) respectively.	$T_a = 288$ K and $u = 3.6$ ms^{-1} Spatial distribution of T_R, from satellite imagery at 13:00 UTC as shown in Figure 6(b). Spatial distribution of z_H and λ_F as shown in Figure 7(a) and (b)
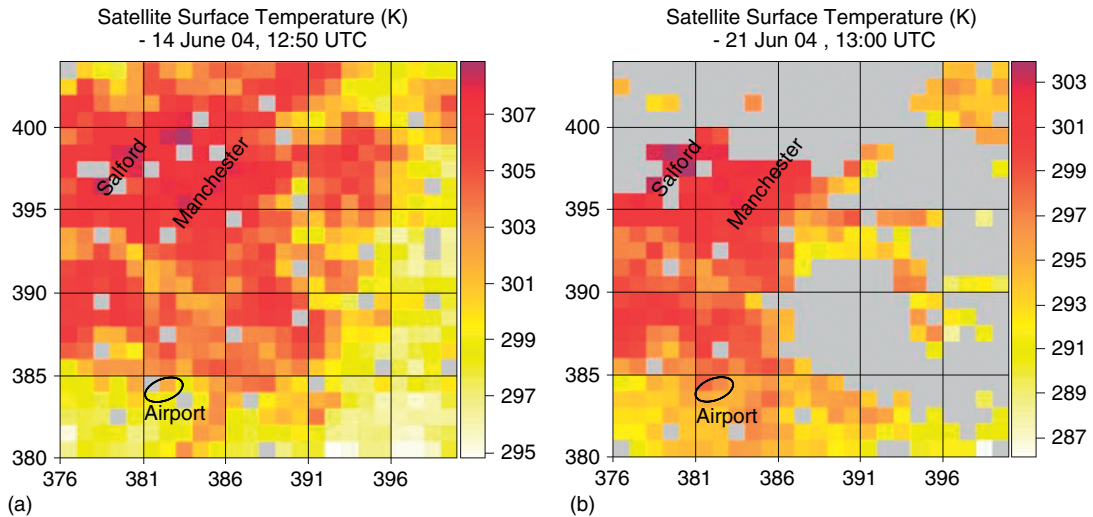
Figure 6. Radiometric surface temperature, T_R, over Greater Manchester (24×24 km), from satellite imagery around 13 UTC, on the study days of 14 (a) and 21 June 2004 (b). The legend on the right-hand sides refers to the values of the temperature expressed in K. The coordinates X and Y are the UK National Coordinates. The total study area is 24×24 km^2 and the area of each grid square is 1 km^2. The locations of Salford and Manchester airport are indicated, and the grey areas are either missing data due to the mapping technique or areas of clouds.
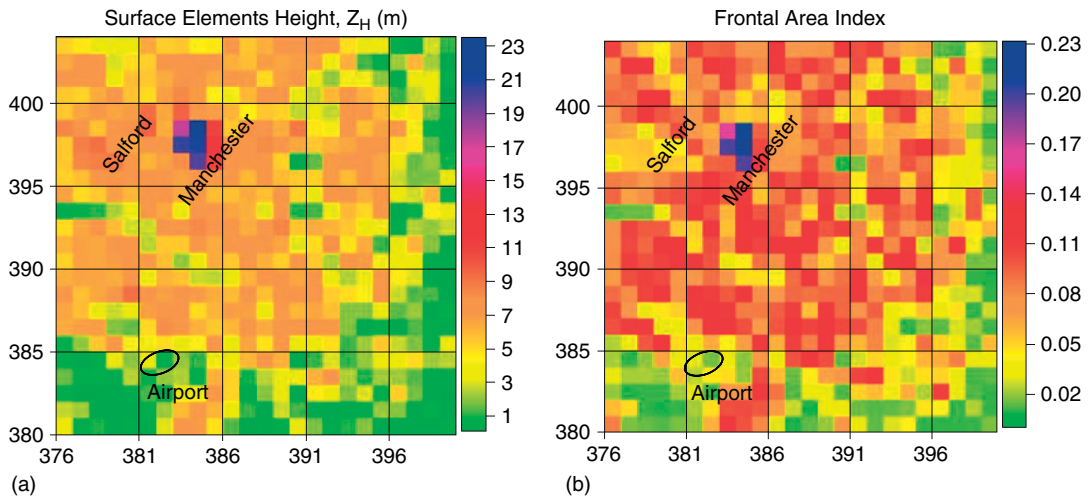
Figure 7. Roughness data for the Greater Manchester study area shown in Figure 6. (a) Mean building height, z_H. The legend on the right-hand side refers to the values of z_H expressed in m. (b) Mean frontal area index, λ_F, for the same study area. The legend on the right-hand side refers to the values of λ_F. Note the difference between the rural areas to the east and south compared to the urban areas. The area of high-rise buildings is clearly evident.

4.2. Model analyses

Figure 8 shows the model results for the spatial distribution of surface sensible heat fluxes at $z_S = 45$ m, Q_H, over a Greater Manchester selected area, on the 14 June 2004 at 1250 UTC and on the 21 June 2004 at 1300 UTC. The input values used in these case studies are described in the previous paragraphs and summarized in Table I.

As expected, higher values of sensible heat flux were found over urbanized zones than over rural zones. The spatial distribution of the model estimates of sensible heat flux follows the same pattern as the surface temperature and roughness, expressed by the parameters z_H, z_D, z_{0M} and λ_F (Figures 6, 7 and 9).

Figure 9(a) and (b) shows the model estimates of the zero-plane displacement length, z_D, and roughness length for momentum, z_{0M}, over the study area, derived from the values of z_H and λ_F shown in Figure 7. These are surface roughness parameters characteristic of the study area and the same for both study days.

Note that using the roughness values over the entire study domain, it can be found that $z_D = 5.3\, z_{0M}$, $z_D = 0.42\, z_H$, $z_{0M} = 0.08\, z_H$. These results are in agreement with those previously published (e.g., Grimmond and Oke, 1999).

Momentum and heat transfer from vegetation and rigid obstacles are significantly different. The transfer of heat to, or from, a surface encounters more aerodynamic resistance than momentum. The excess resistance for heat is expressed commonly in terms of the dimensionless parameter kB^{-1}, which is a term of Equation (2):

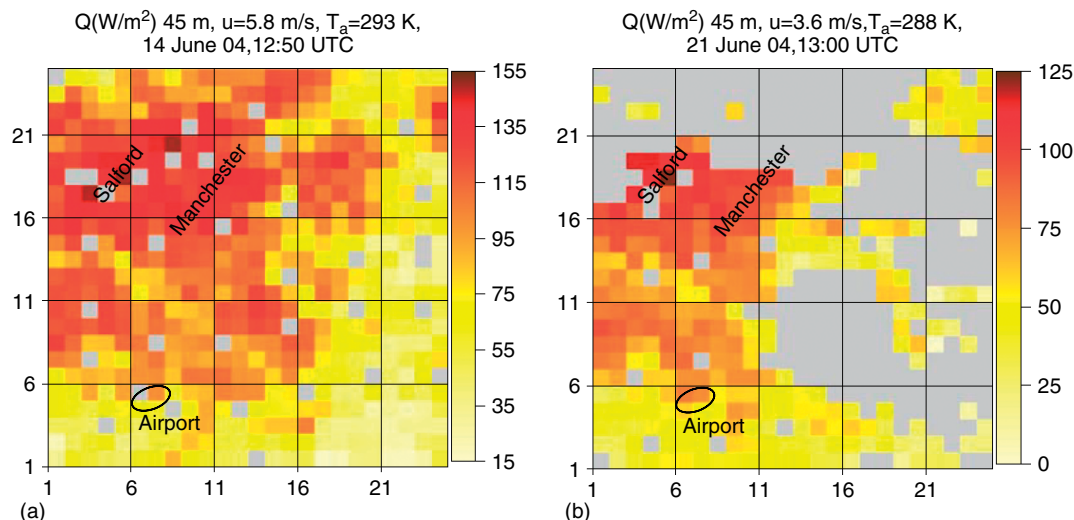$$kB^{-1} = \ln\left(\frac{z_{0M}}{z_{0H}}\right) \tag{5}$$

Figure 8. Model estimates of surface sensible heat flux, Q_H, on 14 (a) and 21 (b) June 2004 around 1300 UTC, for the Greater Manchester study area (24×24 km²) shown in Figure 6. The legend on the right-hand side refers to the values of Q_H expressed in W m⁻², and the grey areas are either missing data due to mapping technique or areas of cloud.
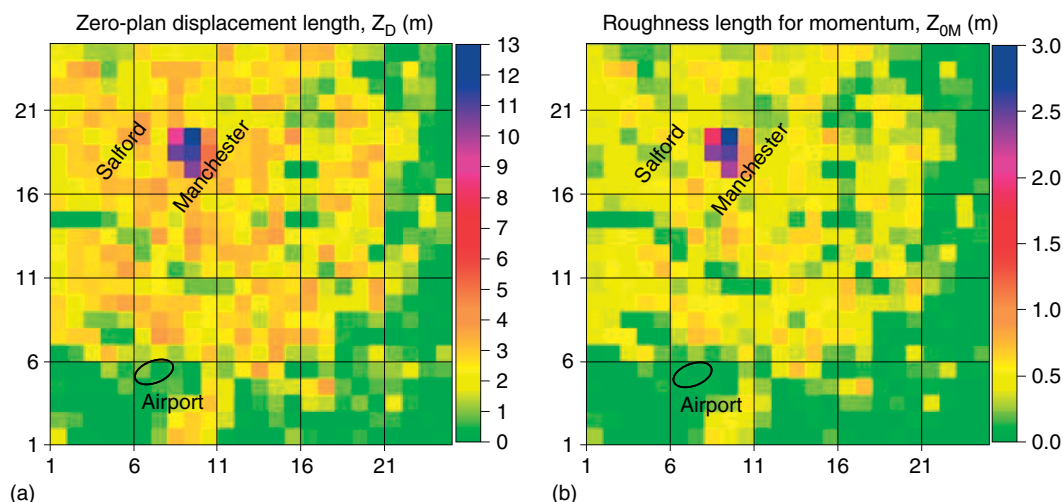

Figure 9. Roughness parameters, zero-plane displacement height and roughness height for momentum, z_D and z_{0M}, for the Greater Manchester study area shown in Figure 6.

Figure 10 shows model estimates of z_{0H}, for the case studies, on 14 and 21 June 2004 around 1300 UTC, for the study area of Greater Manchester. These values are related with the model results of sensible heat flux shown on Figure 8.

Figure 11 shows model results of $kB^{-1} = \ln(z_{0M}/z_{0H})$ for the two case studies. These values are calculated from z_{0M} and the model estimates z_{0H} shown in Figures 9(b) and 10.

Taking into consideration the two case studies, it is found that z_{0H} values range between $\sim 10^{-21}$ and $\sim 10^{-2}$, with the lower values sited over urbanized zones and the highest values over rural areas. Values between 10^{-9} and 10^{-15} occur in the urbanized zones, except for the city centre, where extremely low values ranging from $\sim 10^{-15}$ to $\sim 10^{-21}$ can be found.

The corresponding model estimates of kB^{-1} over urbanized zones lie on a range of values of $15-30$ over

the urbanized zones, but in the city centre these values can be very high, around 50. The lowest values of kB^{-1} are found over the rural zones.

These values of z_{0H} and kB^{-1} are in the range of the values referred to in the published literature.

Voogt and Grimmond (2000), in a study of a simple urban area found extremely small radiometric roughness lengths for heat (z_{0H}), ranging from 10^{-4} to 10^{-12} m. The authors admit that this small value suggests that similarity theory is predicting physically unrealistic values to compensate for the inadequacy of the stability dependence of the exchange coefficient or aerodynamic resistance (as documented previously by Sun and Mahrt, 1995). They note that these small values have also been found by others, e.g., Sugita and Brutsaert (1990) and Malhi (1996). The authors suggest that the values in their study are likely to be close to the extreme because of the lack of vegetation at the site. Voogt and Grimmond (2000)
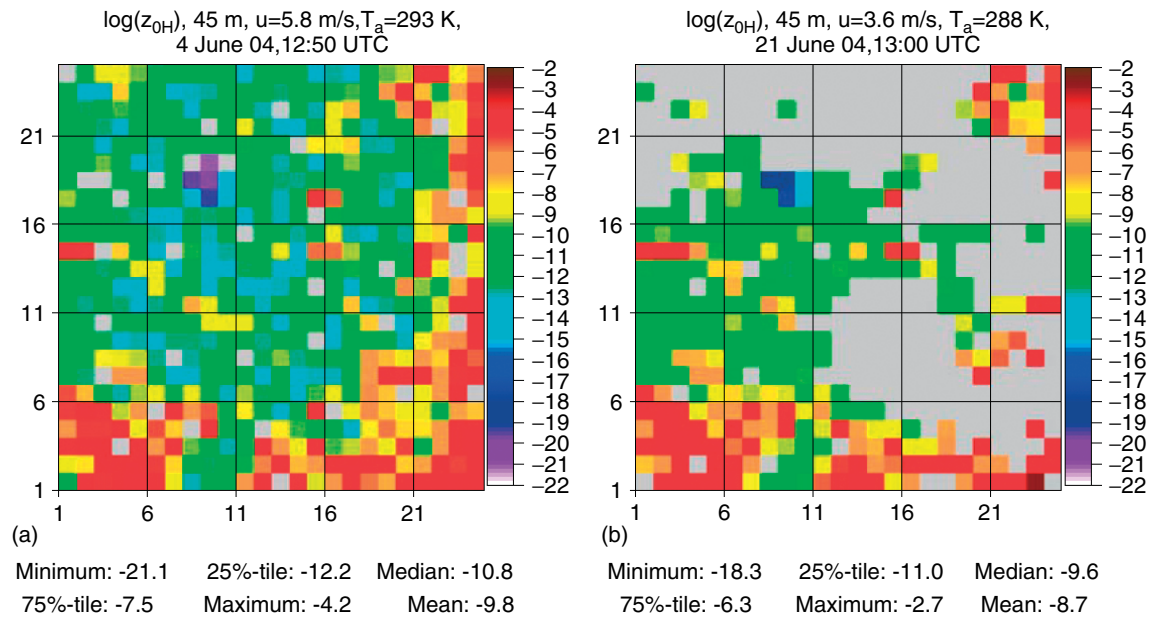
Figure 10. Model estimates of $\log(z_{0H})$ for the case studies, on 14 (a) and 21 (b) June 2004 around 1300 UTC, for the Greater Manchester study area (24×24 km^2). These estimates are related to the model results of sensible heat flux shown in Figure 8. Statistics over the entire study domain, for the model estimates of $\log(z_{0H})$ are shown at the bottom of the figures. Grey areas are as in Figure 8.
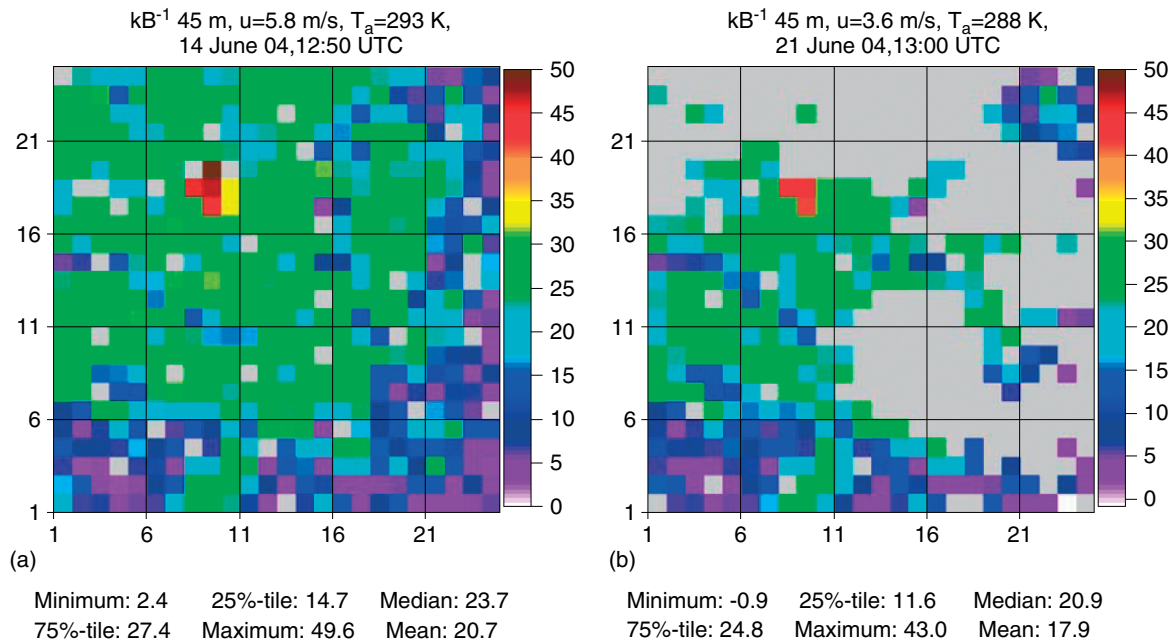

Figure 11. Model estimates of kB$^{-1} = \ln(z_{0M}/z_{0H})$ on the 14 (a) and 21(b) June 2004 around 1300 UTC, for the Greater Mancheste study area (24×24 km^2). These values are related to the model results of sensible heat flux shown in Figure 8. Statistics over the entire study domain, for the model estimates of kB^{-1} are shown at the bottom of the figures. Grey areas are as in Figure 8.

conclude that, for the studied urban environment, a reasonable estimate for kB^{-1}, appears to be about 20–27, which is larger than those observed over vegetated and agricultural surfaces and suggests extremely small z_{0H} values. This range represents the results obtained by three independent methods. The values determined for the bluff-rough curve (Brutsaert, 1982) provide the largest values and are used in the present study (Section 2).

4.3. Testing the impact of roughness heterogeneity

In order to evaluate the impact of the roughness differences on the spatial distribution of Q_H, the model has been run using the same parameters over the entire study domain, except for the roughness which has the spatial distribution shown in Figure 9. Here, the value used as the model input for T_R is the mean satellite radiometric surface temperature observed over the study
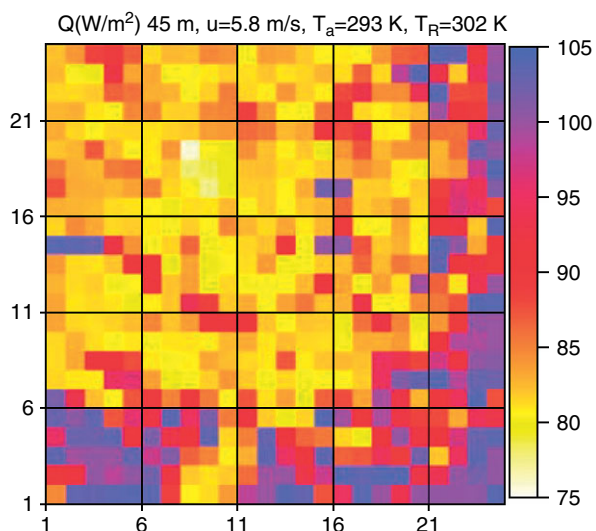
Q(W/m^2) 45 m, u=5.8 m/s, T$_a$=293 K, T$_R$=302 K

Figure 12. Model estimates of sensible heat flux, Q_H, over 24×24 km^2, using as inputs the values presented on the top of the graph. Namely, $z_S = 45$ m, $T_R = 302$ K (29 °C), $u = 5.8$ ms^{-1}, $T_a = 293$ K (20 °C), with the z_H and λ_F spatial distributions of Figures 7(a) and 1(b), respectively.

domain at 1250 UTC ($T_R = 302$ K), and is taken to be the same over the entire study domain. Also, the values for the wind speed, $u = 5.8$ ms^{-1}, and the air temperature, $T_a = 293$ K, are considered to be the same in all the domain cells. Results for the spatial distribution of sensible heat flux, Q_H, over Greater Manchester based on the situation of 14 June 2004 at 1250 UTC are shown in Figure 12.

The test performed to evaluate the impact of roughness on the spatial distribution of Q_H (compare Figure 12 with Figure 9(a) and (b)) shows that, although the patterns of Q_H and z_{0M} (or z_D) are similar, the values of Q_H are lower where the roughness is higher!

A comparison of Figures 12 and 7(b) reveals that the fields shown have a similar pattern. However, higher

values of the surface sensible heat flux, Q_H, occur in the urban sectors with relatively lower surface roughness, λ_F, and vice versa. This result is in agreement with the basic model equations, and with the model test results, presented in Sections 3.1 and 3.2 of this paper. This is due to the fact that the λ_F values over the entire study area are less than the threshold value of 0.29. As pointed out in Section 3.1 (Figure 1), while $\lambda_F < 0.29$, z_{0M} increases and Q_H decreases as λ_F increases. However, there is different behaviour of the roughness parameter z_{0M} for values of $\lambda_F > 0.29$. The physical meaning of this threshold was mentioned in Section 3.1, namely that above this value 'over sheltering' occurs.

5. Initiation of convection

In unstable conditions, updrafts are associated with an increase in temperature and sensible heat flux associated with the upward movement of buoyant thermals. The sensible heat flux is a measure of the vertical gradient of temperature and the lapse rate given the equivalent thermal forcing on the atmosphere (e.g. Oke, 1987). Hence, the field of sensible heat flux relates to the occurrence of upward moving thermals in unstable conditions and therefore the likely initiation of rainfall in near saturated conditions. We next examine this in relation to the urban area of Greater Manchester.

Figure 13 shows the surface pressure field and frontal positions over the United Kingdom and surrounding areas at 1200 UTC on 21 June 2004. Convective cells are shown to be moving across North West England in the MODIS visible satellite image during late morning on 21 June 2004 (Figure 14).

In order to examine the rainfall from the convective cells, data from the C-band Hameldon Hill radar (Figure 15) located some 24 km north of the city centre are displayed in Figure 16 on Hovmoller diagrams. In these diagrams, the distance is plotted against time for a
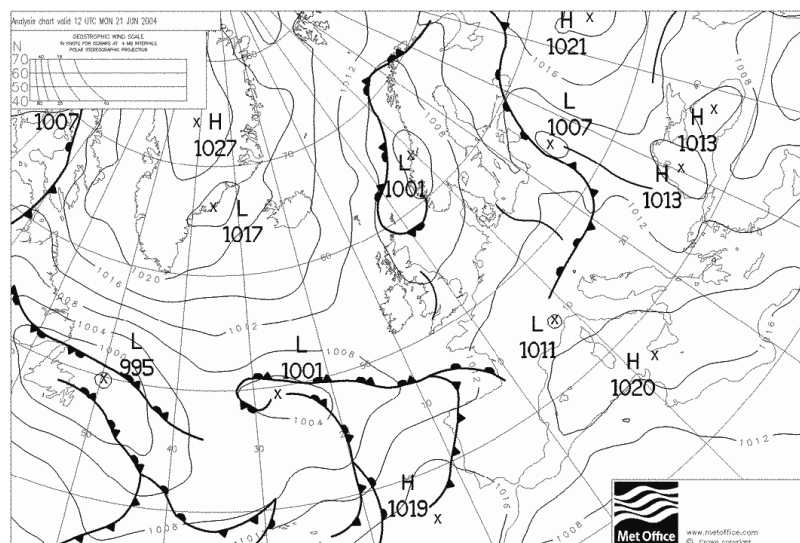

Figure 13. The synoptic pressure field and frontal positions over the United Kingdom and surrounding area at 1200 UTC on 21 June 2004.
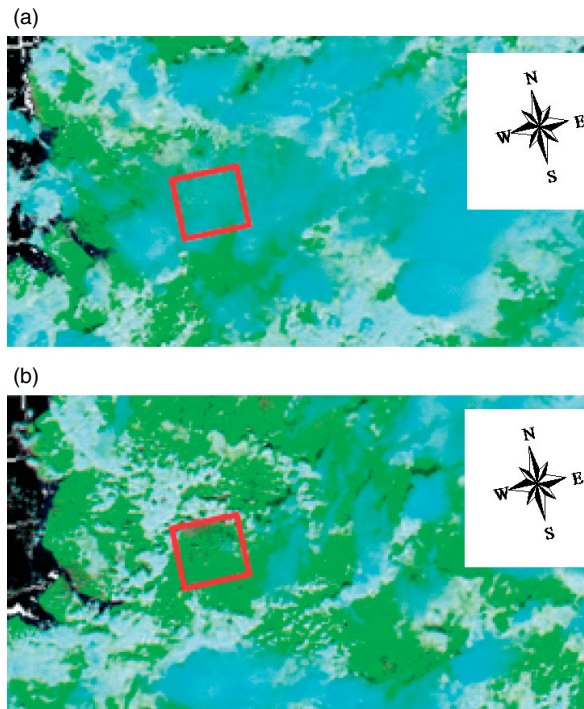
(a)

(b)

Figure 14. Satellite images over England on 21 June 2004 (MODIS, Bands 7-2-1, 5 min, 500 m) (a) Terra/MODIS, 1115 UTC (b) Aqua/MODIS, 1300 UTC. The red line delimits the Greater Manchester study area of 24×24 km^2. Note that there are slight differences in the projection between (a) and (b).
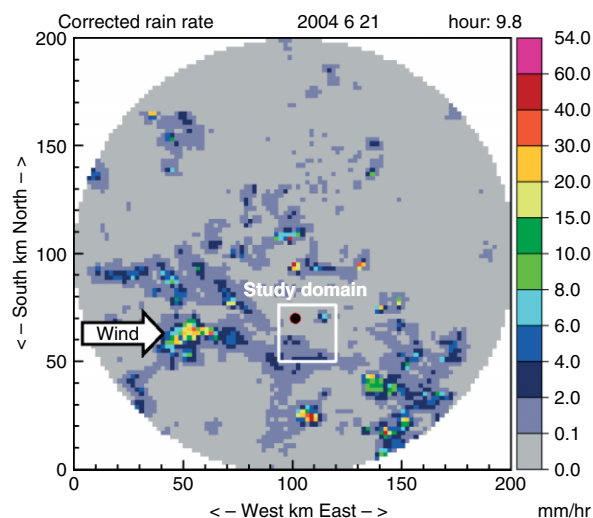

Figure 15. Rainfall rate (mm h^{-1}) on 21 June 2004, around 0948 UTC, given by the Hameldon Hill C-band radar located some 24 km north of the centre of Manchester, North West England. The red and white dot indicates the Manchester city centre. This image is an example of the radar product used in this work (10-min image, with 2×2 km^2 spatial resolution).

direction corresponding to the low wind level direction (westerly in this case).

Figure 16(a) shows the diagram constructed for the period 0600–1100 UTC on 21 June 2004, Figure 16(b) shows the same format for the period 1200–1700 UTC on this day. The colours indicate the rainfall rates

in mm h^{-1}, and the centre of each box ($y = 0$ km) corresponds to the centre of the urban area of Greater Manchester.

During the morning (Figure 16(a)), a convective cell is generated just downwind of Manchester city centre moving in an easterly direction. In addition, cells are also seen to form on the western edge of the urban area, dissipating as they more over to the east of the city towards the upland area. In the afternoon (Figure 16(b)), a cell forms to the west of Manchester city centre over Salford moving eastwards and dissipating.

The areas associated with the cell generation seem to be those areas in which the sensible heat flux is largest (Figure 8) brought about by the existence of high-rise buildings. Baik *et al.* (2001) carried out a numerical study of dry and moist convection forced by an urban heat island. They found that the distance downwind where rain formed depended upon the strength of the surface heating amplitude, the wind speed and the relative humidity. For a heating amplitude of 2 W kg^{-1}, a wind speed of 5 m s^{-1}, and 90% relative humidity, rain occurred some 58 km downwind of the location of the maximum heating. The heat amplitude *equivalent* to the sensible heat flux maximum shown in Figure 8 (about 120 W m^{-2}) is about 6 W kg^{-1}, assuming a mean canopy layer depth of 20 m. Given near saturated conditions, one might therefore expect rain to develop much closer to the source of the maximum heating equivalent. Indeed, in Figure 16, occurrence of rain is first noticed some 10 km downwind of Salford in the morning of the 21 June 2004. In the afternoon, the rain first occurs over Salford, implying that the convection may be first initiated over the upwind rural–urban boundary, or the high-rise buildings lead to significant upward vertical velocities. It would appear that the area of Salford (high-rise buildings close together) has a similar impact to medium-height buildings over a larger area, as predicted by the experiments reported in Section 3.2 Which of these areas leads to convective cell generation depends upon the details of the wind and temperature fields.

6.   Concluding remarks

The sensitivity of Q_H to the different model parameters, T_R, T_a, u, z_H and λ_F, has been investigated. Initial experiments aimed at examining the impact of spatial variations of roughness and stability have shown that significant variations in sensible heat flux may occur. Such variations may lead to the initiation or enhancement of convection when the boundary layer is unstable and near saturation.

In our study, the main objective was to apply the model to convective daytime summer conditions. These are conditions for which we anticipated that the urban morphology would modify the sensible heat flux, and influence convective developments. For the range of typical input values used, the model behaves reasonably for slightly stable to unstable conditions, but, as expected, it fails for stable conditions.
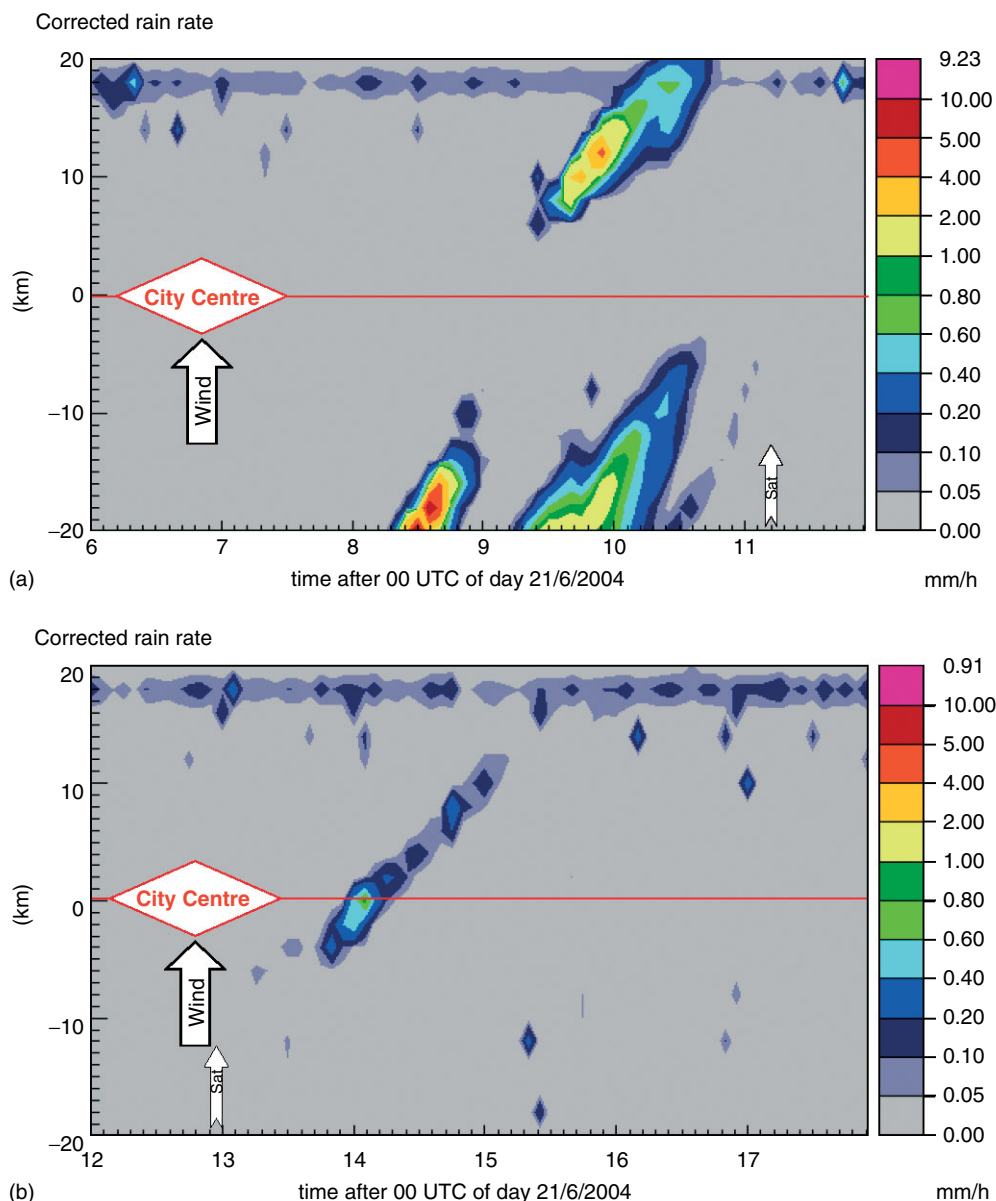
Figure 16. Hovmoller diagrams of the rainfall rate (mm h^{-1}) on 21 June 2004 derived from the Hameldon Hill C-band radar located some 24 km north of the centre of Manchester, North West England (a) 0600–1100 UTC and (b) 1200–1700 UTC. The coordinates represent distance along a 7-km wide swath running through the city centre in the direction of the westerly cell movement and the abscissa represents time. Some small spurious areas of rain remain where the removal of radar ground clutter echoes has been incomplete. The time of the satellite images shown in Figure 14 are indicated by the vertical arrows next to the time axis.

A case study was described in which the model-generated distribution of sensible heat flux over Greater Manchester was compared with rainfall fields derived from C-band radar. Convective cells are observed to initiate just downwind of the centre of the city occupied by high-rise buildings, the exact impact of the building configuration depending upon the details of the wind and temperature fields.

References

Baik J-J, Kim Y-H, Chun H-Y. 2001. Dry and moist convection forced by an Urban Heat Island. *Journal of Applied Meteorology* **40**: 1462–1475.

Brutsaert WH. 1982. *Evaporation into the Atmosphere*, 2nd edn. D. Reidel: Doordrecht, Holland; 299.

Carraça MGD, Collier CG. 2006. An urban surface database of morphologic parameters for use in atmospheric boundary layer

modelling. Submitted to *Computers, Environment and Urban Systems*.

Collier CG. 2006. The impact of urban area on weather. *Quarterly Journal of the Royal Meteorological Society* **132**: 1–25.

Dyer AJ. 1974. A review of flux-profile relationships. *Boundary Layer Meteorology* **7**: 363–372.

Ellefsen R. 1990–1991. Mapping and measuring buildings in the canopy boundary layer in ten U.S. cities. *Energy and Buildings* **15–16**: 1025–1049.

Fisher B. 2002. Meteorology applied to urban air pollution problems. Draft Progress Report April 2002. [http://www.dmu.dk/Atmospheric-environment/cost/docs/Cost715_progress.pdf].

Grimmond CSB, Oke TR. 1999. Aerodynamic properties of urban areas derived from analysis of surface form. *Journal of Applied Meteorology* **38**: 1262–1292.

Grimmond CSB, King TS, Roth M, OKE TR. 1998. Aerodynamic roughness of Urban Areas derived from Wind Observations. *Boundary Layer Meteorology* **89**: 1–24.

Guo X, Fu D, Wang J. 2006. Mesoscale convective precipitation system modified by urbanization in Beijing City. *Atmospheric Research* **82**: 112–126.

Högström U. 1988. Non-dimensional wind and temperature profiles in the atmospheric surface layer: A re-evaluation. *Boundary Layer Meteorology* **42**: 55–78.

Malhi Y. 1996. The behaviour of the roughness length for temperature over heterogeneous surfaces. *Quarterly Journal of the Royal Meteorological Society* **122**: 1095–1125.

Oke TR. 1987. *Boundary Layer Climates*, (2nd edn). Routledge: London; 435.

Paulson CA. 1970. The mathematical representation of wind speed and temperature profiles in the unstable atmospheric surface layer. *Journal of Applied Meteorology* **9**: 857–861.

Raupach MR. 1994. Simplified expressions for vegetation roughness length and zero-plane displacement as functions of canopy height and area index. *Boundary Layer Meteorology* **71**: 211–216.

Raupach MR. 1995. Corrigenda. *Boundary Layer Meteorology* **76**: 303–304.

Rozoff CM, Cotton WR, Adegoke JO. 2003. Simulation of St. Louis, Missouri, Land use Impacts on Thunderstorms. *Journal of Applied Meteorology* **42**: 716–738.

Segal M, Arrit RW. 1992. Nonclassical mesoscale circulations caused by surface sensible heat flux gradients. *Bulletin of the American Meteorological Society* **73**: 1593–1604.

Shaw EM. 1962. An analysis of the origins of precipitation in Northern England, 1956–1960. *Quarterly Journal of the Royal Meteorological Society* **88**: 539–547.

Shepherd JM. 2002. An investigation of the influence of urban areas on rainfall using a cloud-mesoscale model and the TRMM satellite. *Proceedings of the Fourth Symposium on the Urban Environment*. American Meteorological Society: Boston; 1–2, Norfolk, VA; 20–24, May 2002.

Shepherd JM. 2005. A review of current investigations of Urban-Induced rainfall and recommendations for the future. *Earth Interactions* **9**: 1–27.

Shepherd JM, Pierce H, Negri AJ. 2002. Rainfall modification by Major Urban Areas: Observations from Spaceborne rain radar on the TRMM satellite. *Journal of Applied Meteorology* **41**: 689–701.

Sugita M, Brutsaert W. 1990. Regional fluxes from remotely sensed skin temperature and lower boundary layer measurements. *Water Resources Research* **26**: 2937–2944.

Sun Y, Mahrt L. 1995. Determination of surface fluxes from the surface radiative temperature. *Journal of the Atmospheric Sciences* **52**: 1096–1106.

Thielen J, Gadian A. 1997. Influence of topography and urban heat island effects on the outbreak of convective storms under unstable meteorological conditions: a numerical study. *Meteorological Applications* **4**: 139–149.

Thielen J, Wobrock W, Gadian A, Mestayer PG, Creutin J-D. 2000. The possible influence of urban surfaces on rainfall development: a sensitivity study in 2D in the meso-γ-scale. *Atmospheric Research* **54**: 15–39.

van Ulden AP, Holtslag AAM. 1985. Estimation of atmospheric boundary layer parameters for diffusion applications. *Journal of Climate and Applied Meteorology* **24**: 1196–1207.

Voogt JA, Grimmond CSB. 2000. Modeling surface sensible heat flux using surface radiative temperatures in a simple Urban area. *Journal of Applied Meteorology* **39**: 1679–1699.

Wieringa J. 1993. Representative roughness parameters for homogeneous terrain. *Boundary Layer Meteorology* **63**: 323–363.